



Multi-objective optimisation based on reliability analysis of a self-propelled capsule system

Jiapeng Zhu · Maolin Liao  · Yang Zheng · Shikun Qi · Zhi Li · Zijin Zeng

Received: 22 November 2021 / Accepted: 12 March 2022 / Published online: 7 April 2022
© Springer Nature B.V. 2022

Abstract In order to promote the stability of a self-propelled capsule moving in digestive tract, the target moving speed, the minimal impact force and the minimal energy consumption are considered as the optimisation objectives simultaneously. The uncertainty of small intestine environment is described by varying the external friction coefficient of capsule. Under such circumstances, NSGA-II, Monte Carlo, and Six-Sigma algorithms are combined to conduct the multi-objective optimisation of both the control and structure parameters based on reliability analysis. Compared with the passive capsules which can only move in one direction relying on small intestine peristalsis, the bi-directional motion can be fulfilled by the self-propelled capsule via adjusting its optimisation parameters. According to the obtained optimisation result, the forward motion of the capsule can achieve a large scale of moving speeds; however, it is difficult for the capsule moving backward with high speed. The reliabilities of both the energy consumption and the impact force can reach 100% via reliability optimisations; however, the reliability of the target moving speed of capsule is hard to be promoted up to 90%. Both the optimisation method and the optimisation result introduced in the paper are expected to be benefit to the improvement of the

self-propelled capsule system and its application in wireless endoscope.

Keywords Self-propelled capsule · Multi-objective optimisation · Reliability analysis · Bi-directional motion

1 Introduction

In recent years, the needs for endoscopic surgery to diagnose gastrointestinal (GI) diseases, such as cancers, ulcers and inflammatory bowel diseases, have increased considerably. In recent times, the majority of GI examinations are still based on wired endoscope, whose foreign body sensation caused by the checking pipeline carrying the probe moving in digestive tract often makes the patient unbearable, hence anesthesia before endoscopic surgery is inevitable. To address the problem, capsule endoscope was introduced into clinical practice about 20 years ago, whose movement in digestive tract mainly depends on GI peristalsis, and thus its moving speed is variable and uncontrollable, making the corresponding examination duration unpredictable. Therefore, a controllable self-propelled capsule endoscope is viewed as the new direction.

One of the major advances in GI examination was the pioneering work in the field of controllable capsule endoscope done by Liu et al. [1–3], specifically, an untethered, self-propelled, controllable capsule

J. Zhu · M. Liao (✉) · Y. Zheng · S. Qi · Z. Li · Z. Zeng
School of Mechanical Engineering, University of Science and Technology Beijing, Beijing 100083, China
e-mail: liaomaolin@ustb.edu.cn

was designed to carefully and reliably examines areas of interest in real time. Based on the effective control of moving speed, the self-propelled capsule can reduce the duration of examination, thus improving the efficiency of endoscopy. The principle of the proposed self-propelled technology is to realise the linear movement of the capsule via the interaction and collision between the periodically driven inner oscillator and the capsule body in the presence of external resistance. This system demonstrates its advantages both in its simplified mechanical design and in its capacity of independent movement in complex small intestine environment without external drive accessories. In this case, many of the complications and risks associated with external arms or propellers, e.g. [4, 5], can be avoided.

The moving efficiency, energy consumption, comfort level of a self-propelled capsule significantly depends on its structure, excitation, and means of propulsion. The structural optimisation was primarily considered by Yan et al. [6] and Liao [7], where the capsule systems with one-sided and two-sided constraints were compared. It was found that the capsule with one-sided constraint can offer a higher moving efficiency, while the one with two-sided constraint can be beneficial for the bi-directional motion of the capsule. Tian et al. [8] studied the interactions between a moving capsule and small intestine by finite element method, to discuss the influence of the structure of digestive tract on the moving speed of a self-propelled capsule. Yan et al. [9] also optimised the geometry of capsule shell of such a vibro-impact system in fluid pipeline to reduce the drag and lift coefficients, and thus improving the locomotive performance of the capsule. Subsequently, the optimisation of the excitation parameters, e.g. the excitation frequency and amplitude, was taken into consideration to improve the progression efficiency of the capsule system; since, for the typical vibro-impact systems [10–14], both the frequency and amplitude of excitation are the two main control parameters to promote the working efficiency. Once the external excitation of the capsule system adopts the square wave signal [1], the duty cycle ratio of the square wave can be viewed as the third control parameter. By varying these parameters, Guo et al. [15] provided the basic understandings of the nonlinear behavior of such piece-wise smooth systems under collision and friction, and further optimised the impact force from

the capsule to improve patient's discomfort [2, 16]. In order to achieve both a higher progression speed and less impact force simultaneously, the optimisation of the excitation parameters was carried out by means of path-following techniques [17]. It was found that by using a proper combination of the three excitation parameters, the collision between the inner oscillator and the capsule can be avoided to eliminate the impact force while keeping the capsule's progression speed up to 14.4 mm/s. In addition, the means of propulsion can also be optimised. Jiang and Xu [18] investigated the locomotion driven by sine-squared strain wave in a linear resistance medium. Zhan et al. [19] considered the vibration driven mechanism. Zhang et al. [20] learned from the earthworm's locomotion mechanism, i.e., retrograde peristalsis wave, and designed the corresponding propulsion method. All of their ideas can also be benefit for designing the self-propulsion of the capsule.

However, all these listed optimisations have focused on one specific parameter and the optimisation objective is also single. They neither considered the interactions of both the structure parameters and the excitation parameters, nor considered the multiple contradictory optimisation objectives which needed to be satisfied simultaneously. In addition, the previous optimisations lacked reliability analysis of both the parametric perturbations and the environmental uncertainties, which are considered to be significant in complex environment, such as the digestive tract. When facing the similar challenge, Liao et al. [14] conducted an optimisation design of an offshore drilling pipe system by integrating the reliability analysis into multi-objective optimisation. In that case, the Isight software [21–24] was used, in which the Six-Sigma algorithm [25–28] was applied to drive the genetic algorithm to conduct multi-objective optimisation, and the obtained optimal solution was then transferred to the Monte Carlo algorithm [29–31] for further reliability analysis under the perturbations of the optimisation parameters. In addition, as an effective algorithm for multi-objective optimisation, NSGA-II [32, 33] was applied by Diao et al. [34] to develop the bi-objective optimisation framework of a vibration-driven locomotion robot. Zhan et al. [35] applied the NSGA-II algorithm to design the locomotor gaits, in which the advantages of NSGA-II in coordinating contradictory optimisation objectives were demonstrated. Based on the above analyses, the

Six-Sigma algorithm, NSGA-II algorithm, and Monte Carlo algorithm will be combined to conduct the multi-objective optimisation with reliability analysis when considering both the parametric fluctuations and the environmental uncertainties.

The rest of the paper is organised as follows. Section 2 introduces the mathematical modelling of the self-propelled capsule system briefly; moreover, the influences of the uncertain friction coefficient of the small intestine environment on the dynamic responses of the capsule system are investigated via bifurcation analysis. Then the three optimisation objectives are proposed in Sect. 3, and the sensitivity analyses of 13 structure and control parameters are conducted to determine the key parameters. In Sect. 4, both the multi-objective optimisation using NSGA-II algorithm and the verification of reliability using Monte Carlo algorithm are introduced. Thereafter, the multi-objective optimisation with reliability analyses of the forward and backward motions of the capsule are conducted in Sects. 5 and 6, respectively. Finally, concluding remarks are provided in Sect. 7.

2 Mathematical model of the self-propelled capsule system

2.1 Dynamic modelling

Conceptual design and physical model of the self-propelled capsule system are presented in Fig. 1, where m_1 and m_2 are the masses of the inner oscillator and the capsule shell, respectively. k and c represent the stiffness of the adjusting spring connecting the oscillator and the capsule and the damping coefficient

led by the relative speed between the capsule and the oscillator, respectively. The springs with stiffness k_1 and k_2 represent the primary and the secondary constraints, and their gaps between the oscillator and the constraints are e_1 and e_2 , respectively. x_m and x_c are the displacements of the oscillator and the capsule, and their velocities are v_m and v_c , respectively. The friction between the capsule and digestive tract is modeled as a Coulomb friction f_c with the friction coefficient μ . The input excitation on the inner oscillator f_e is a square wave signal modulated by the amplitude P_d , the period T and the duty cycle ratio d , where the duty cycle ratio is the fraction of one period in which the on-off excitation is active.

The capsule system moves as the forward and backward stick-slip modes which include the following four phases: *stationary capsule without impact*, *moving capsule without impact*, *stationary capsule with impact* and *moving capsule with impact*. All these phases can be modelled using the following equations of motion as

$$\begin{cases} m_1 \ddot{x}_m = f_e - f_i, \\ m_2 \ddot{x}_c = f_c + f_i, \end{cases} \tag{1}$$

where f_i represents the interaction force between the capsule and the oscillator written as

$$f_i = \begin{cases} k(x_r + e) + cv_r + k_2(x_r + e_2), & x_r \leq -e_2, \\ k(x_r + e) + cv_r, & -e_2 < x_r < e_1, \\ k(x_r + e) + cv_r + k_1(x_r - e_1), & x_r \geq e_1, \end{cases} \tag{2}$$

where $x_r = x_m - x_c$ and $v_r = v_m - v_c$ represent the relative displacement and velocity between the oscillator

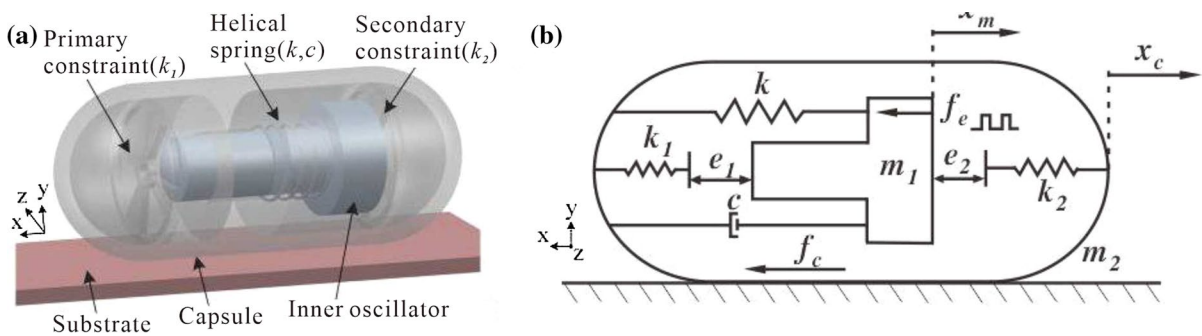


Fig. 1 a Conceptual design and b physical model of the vibro-impact capsule system

and the capsule. e is the precompression of the adjusting spring k . In this study, the friction between the capsule and digestive tract is given as

$$\begin{cases} f_c \in [-P_f, P_f], & v_c = 0, \\ f_c = -\text{sign}(v_c)P_f, & v_c \neq 0, \end{cases} \quad (3)$$

where $P_f = \mu(m_1 + m_2)g$ is the static friction of the capsule system, and g is the gravitational acceleration. The external excitation f_e can be written as

$$f_e(t) = \begin{cases} P_d, & t \in [nT, nT + dT], \\ 0, & t \in (nT + dT, nT + T), \end{cases} \quad (4)$$

where n is the period number, P_d , T and $d \in (0, 1)$ are the amplitude, period and duty cycle ratio of the signal, respectively. To explain, the control signal of capsule in this paper uses square wave signal, which hence needs to be described by the above three parameters. Furthermore, the change of f_i in one period can be expressed as

$$f_i = f_0 + H_{k1}f_1 + H_{k2}f_2, \quad (5)$$

$$\begin{cases} f_0 = k(x_r + e) + cv_r, \\ f_1 = k_1(x_r - e_1), \\ f_2 = k_2(x_r + e_2), \end{cases} \quad (6)$$

$$H_{k1} = \begin{cases} 1, & x_r - e_1 \geq 0, \text{ (contact with } k_1), \\ 0, & x_r - e_1 < 0, \text{ (no contact)}, \end{cases} \quad (7)$$

$$H_{k2} = \begin{cases} 1, & x_r + e_2 \leq 0, \text{ (contact with } k_2), \\ 0, & x_r + e_2 > 0, \text{ (no contact)}. \end{cases} \quad (8)$$

Therefore, the maximum impact force from capsule acting on digestive tract is defined as

$$f_{\max} = \max_{0 < t < T} |f_i|, \quad (9)$$

which should be as low as possible to minimise patient’s discomfort. The average moving speed and the power consumption of the self-propelled capsule during $t \in [N_0T, N_0T + N_aT]$ are defined as

$$V_c = \frac{x_c(N_0T + N_aT) - x_c(N_0T)}{N_aT}, \quad (10)$$

$$P_{\text{avg}} = \frac{1}{N_aT} \int_{N_0T}^{N_0T+N_aT} \frac{U_s^2}{R_s} dt, \quad (11)$$

where N_0 and N_a are the period numbers, U_s is the driven voltage of exciter which can be described as

$$U_s = I_s \cdot R_s = \frac{f_e \cdot R_s}{k_i}, \quad (12)$$

where k_i and R_s are the force–current ratio and the resistance of exciter, respectively. Therefore, P_{avg} can be further expressed as

$$P_{\text{avg}} = \frac{d \cdot R_s \cdot P_d^2}{k_i^2}. \quad (13)$$

In the developed dynamic model, all the structure and control parameters related to the self-propelled capsule are listed in Table 1, which are obtained from the experimental rig developed by Liu et al. [1, 3].

2.2 Analyses of dynamic responses

Based on the developed mathematical model, the dynamic responses of the self-propelled capsule can be analysed by varying the system parameters. In addition, after swallowing, the capsule needs to pass

Table 1 Structure and control parameters of the initially designed capsule

Parameters	Signs	Units	Values
Mass of inner oscillator	m_1	kg	1.8×10^{-3}
Mass of capsule shell	m_2	kg	1.67×10^{-3}
Friction coefficient	μ	1	0.2293
Stiffness of adjusting spring	k	N/m	59.972
Stiffness of primary spring	k_1	N/m	27,900
Stiffness of secondary spring	k_2	N/m	53,500
Precompression of adjusting spring	e	m	0
Gap of primary spring	e_1	m	1.5×10^{-3}
Gap of secondary spring	e_2	m	0
Damping coefficient	c	N s/m	0.0156
Force–current ratio	k_i	mN/A	55
Resistance of exciter	R_s	Ω	0.72
Excitation amplitude	P_d	N	6×10^{-3}
Excitation frequency	f	Hz	30
Duty cycle ratio	d	%	30

through the human esophagus, stomach, small intestine and colon, and finally be excreted through anus. As the most important part, the length of small intestine is 4–6 m, its structure is the most complex, and the detection blind area is the most concentrated. In order to ensure the reliability of the capsule, the jejunum segment of the small intestine is taken as the research object of GI, and unstable friction coefficient is used to define the influence of uncertain environment. As an example, the excitation frequency f is set as the bifurcation parameter to study the variation of the dynamic responses of capsule; moreover, for each frequency case, the friction coefficient μ varies in the range of [0.1, 0.4], which has been measured via experiments [2].

The obtained simulation results are shown in Fig. 2, and the influences of the varied friction coefficients are compared when the excitation frequency is $f = 5, 40$ and 75 Hz, respectively, see the three lists of red dots in subplot (a). In addition, Fig. 2b–m show the time series and phase portraits for different excitation frequencies with different friction coefficients. Specifically, when the excitation frequency is set as low as $f = 5$ Hz, the capsule can basically keep moving forward, however, its moving speed varies from almost 0 mm/s to 15 mm/s, the influence of the varied friction coefficient is of importance. As observed in subplots (b)–(e), the inner oscillator impacts with the primary constraint spring for multiple times, the average moving speed of capsule drops sharply from 13.62 mm/s to almost stationary with the friction coefficient increasing from 0.1 to 0.4. When the excitation frequency is set as moderate as $f = 40$ Hz, the uncertainty of the friction from the small intestine environment changes not only the moving speed of the capsule, but also its moving direction. As shown in subplots (f)–(i), as increasing the friction coefficient from 0.1 to 0.4, the average moving speed of capsule changes from +1.32 mm/s forward to –0.88 mm/s backward; however, the vibration condition of the capsule always maintains as single period motion with single impact between the inner oscillator and the primary constraint spring. When the excitation frequency is set as high as $f = 75$ Hz, the corresponding moving speed of capsule concentrates around 0 mm/s, the influence of the varied friction coefficient is not significant since the input excitation cannot overcome the frictional resistance to push the capsule to move effectively.

According to above analysis, it can be concluded that the accurate motion state of the capsule moving in the uncertain small intestine environment is difficult to be predicted. Under such circumstances, the parameter optimisation of the self-propelled capsule combined with the reliability analysis of the uncertain environmental parameter should be considered to further promote the moving stability of the capsule applied in endoscopy.

3 Optimisation objectives and sensitivity analyses

In order to fulfil the steady movement of the self-propelled capsule with high efficiency in uncertain small intestine environment, a series of practical constraint conditions need to be considered simultaneously. For this purpose, the physical structure of the capsule as well as the controllable internal excitation should be designed properly. Hence, the optimisation of the self-propelled capsule system is necessary; as the first step, both the optimisation objectives and the optimisation parameters should be determined according to the practical constraint conditions.

3.1 Determination of optimisation objectives

Primarily, in order to improve the diagnosing experience of patient, endoscopy procedure is expected to be completed within a short period of time usually within 20 min. Since the equivalent length of intestines is about 8–9 m, the average moving speed of capsule V_c is better to be maintained around 8 mm/s, which can be viewed as the first optimisation objective. As the main advantage of the proposed capsule endoscope, it is equipped with an inner excitation module, which enables the linear motion of capsule based on the impact force from the inner oscillator acting on the capsule shell. However, due to the tiny size of the capsule, whose diameter is around 10 mm with its whole length less than 30 mm, its energy supply unit is extremely limited. Under such circumstances, the lithium button battery is generally used as the power source, however, its energy storage is relatively low. Therefore, the average energy consumption P_{avg} of the self-propelled capsule during operation should be well controlled, which can be proposed as the second optimisation objective. Meanwhile, due to the existence

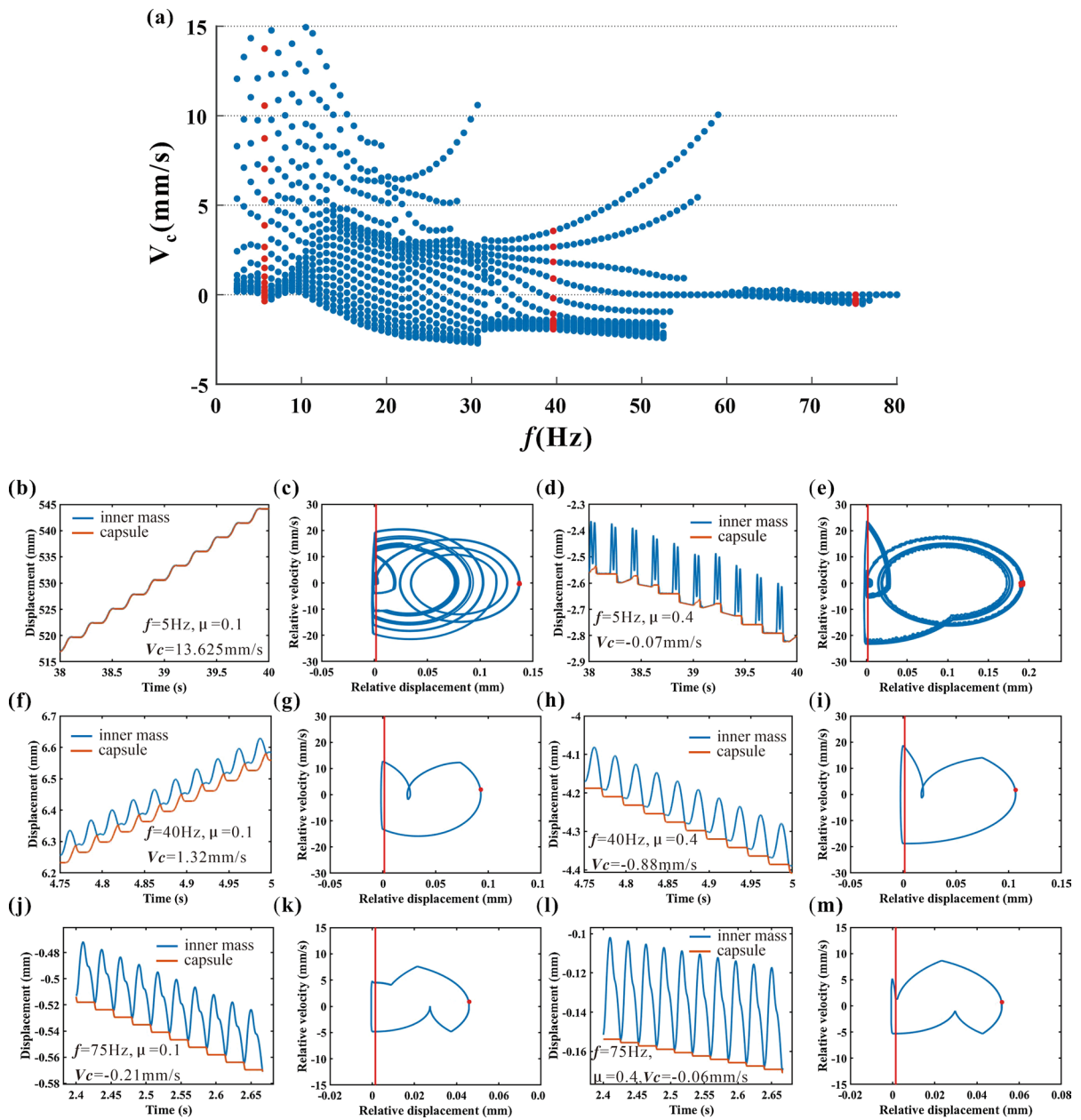


Fig. 2 (Colour online) Bifurcation analysis of the excitation frequency under the varying friction coefficient. Subplot **a** shows the bifurcation diagram, and subplots **b–m** show the

corresponding time series and phase portraits for different excitation frequencies ($f = 5, 40$ and 75 Hz) and friction coefficients ($\mu = 0.1$ and 0.4)

of interactions between the inner oscillator and the capsule shell, the vibration impact of the capsule on the intestines will be triggered, which will directly affect the diagnosing experience of patient. Hence, the impact force from the vibration capsule f_{max} should be minimised, which can be viewed as the

third optimisation objective. Based on above analysis, the optimisation of the self-propelled capsule system is a typical multi-objective optimisation; meanwhile, the optimisation objectives also correspond to the constraint conditions, which are listed in Table. 2.

Table 2 Constraint conditions based on the three optimisation objectives

Objectives	Units	Target	Allowed range
V_c	mm/s	8	[6, 10]
f_{max}	N	Minimum	[0, 0.1]
P_{avg}	W	Minimum	[0, 0.02]

3.2 Sensitivity analyses of optimisation parameters

In addition to the determination of optimisation objectives, both the optimisation parameters and their variation ranges should also be confirmed before performing optimisation. As listed in Table 1, there are 15 quantitative parameters for the self-propelled capsule. Except the force–current ratio (k_i) which is a constant, the other 14 parameters are variable, which can be further divided into two parts: structure parameters and control parameters. According to the different optimisation objective, the influence of different parameter is in different level. Therefore, the sensitivity analyses of all the variable parameters should be conducted to compare their contribution rates for different optimisation objectives. On this basis, the main optimisation parameters can be clarified. Specifically, during the sensitivity analyses, all the 14 parameters are set to fluctuate as $\pm 40\%$ around their initial values listed in Table 1, and then they are combined with each other by using Latin hypercube sampling to generate the design matrix for application of the design of experiment (DOE) method. Based on the statistics of the results for all the simulated 800 parameter combinations, the sensitivities of the 14 parameters are determined, which are illustrated in Fig. 3.

As observed in Fig. 3a, the contribution rates of optimisation parameters on V_c are distributed. Specifically, m_2 owns the greatest negative contribution rate -15.24% on V_c meanwhile, f , e , μ and c also have great influences on V_c , and their contribution rates are all over 10% and negatively related to V_c . Comparatively, the parameters d , e_2 , P_d , R_s , k_1 , and k are positively related to V_c , however, their contribution rates are all less than 7% . The contribution rates on the maximal impact force f_{max} are shown in Fig. 3b, and the parameter that has the greatest contribution rate on f_{max} is e_2 as 38.13% . In addition, the contribution rates of f and k are also larger than 10% , while the influences of other parameters are relatively

small. According to Fig. 3c, the only three parameters related to the average energy consumption of the self-propelled capsule are $P_d = 42.40\%$, $d = 41.94\%$, and $R_s = 14.89\%$, all of which are positively correlated with P_{avg} , hence, all of the three parameters should be limited to small values to secure the low energy consumption of this capsule system.

4 Multi-objective optimisation by NSGA-II

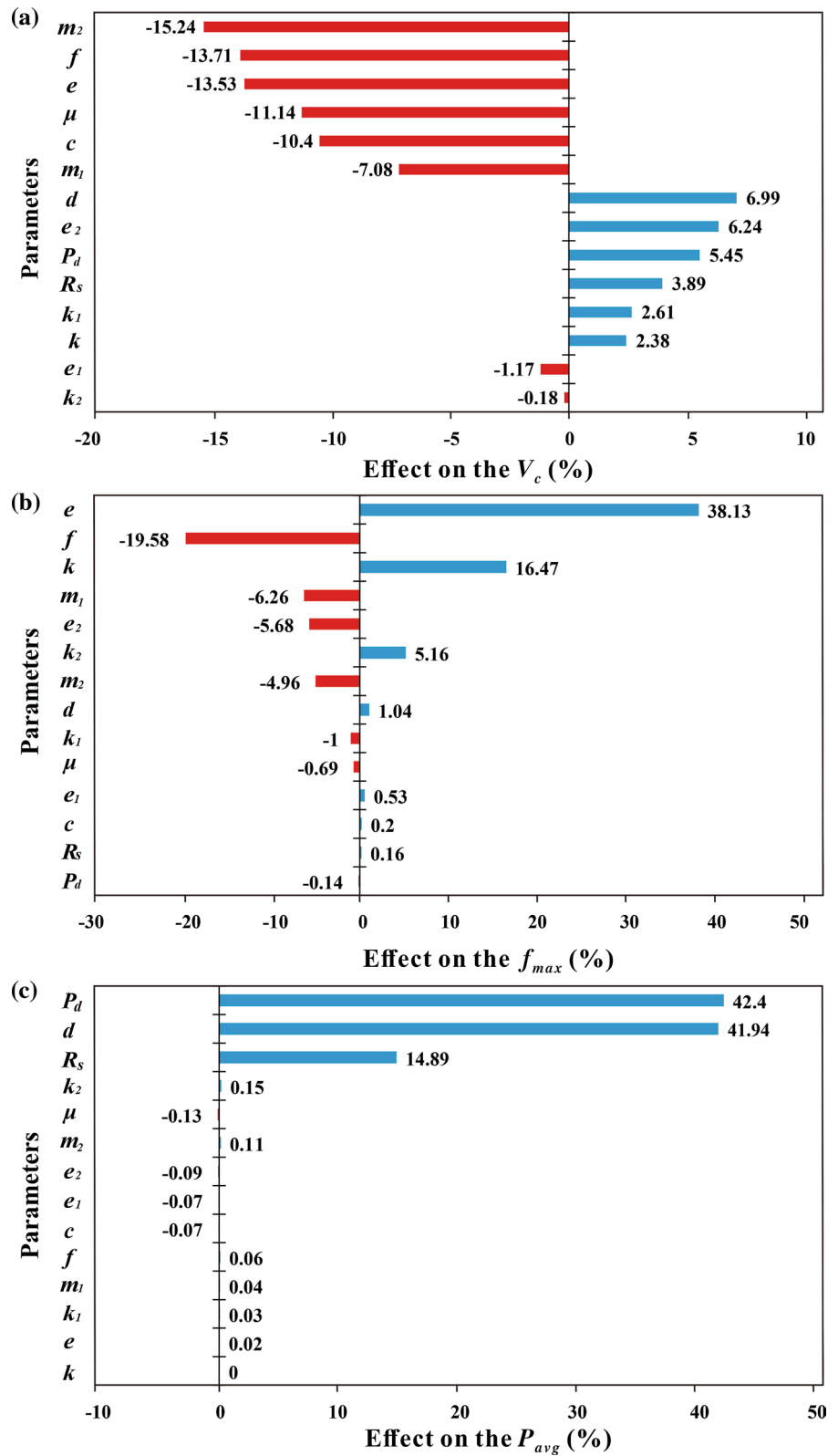
Since both the optimisation objectives and the optimisation parameters have been determined, as the next step, the multi-objective optimisation can be carried out. In this present work, the NSGA-II algorithm is used to conduct the multi-objective optimisation. The superiority of NSGA-II includes the following three parts: primarily, its computational complexity is greatly reduced by fast non-dominated sorting approach; secondly, the congestion degree comparison operator is applied to replace the shared radius, and thus the obtained local optimisation solution can be extended to the whole Pareto domain, hence, the population diversity can be maintained; thirdly, the elite strategy is introduced to expand the sampling space, hence, the loss of the optimisation solution can be prevented, and thus the computing speed and robustness can be promoted. The analysis flow of NSGA-II can be briefly described as Fig. 4.

4.1 Preliminary multi-objective optimisation

As the first taste of multi-objective optimisation of the self-propelled capsule, the environmental parameter μ is set as a constant, while a total of 13 structural and control parameters are applied for optimisation, and their initial values have been given in Table 1; meanwhile, both the structure and control parameters are allowed to fluctuate around their initial values, and their corresponding lower and upper boundaries of variation ranges are listed in Table 3. In particular, the control parameters are set to be adjusted in large ranges to explore the proper combinations, while the structure parameters are limited in relatively small ranges due to the limitations of both the material property and the capsule size.

During the preliminary multi-objective optimisation, the initial population number is set as 100, the number of generations is set as 12, the crossover rate

Fig. 3 Contribution rates of optimisation parameters on the optimisation objectives of **a** V_c , **b** f_{max} , and **c** P_{avg} . The blue bars indicate the positive correlations, the red bars indicate the negative correlations. (Color figure online)



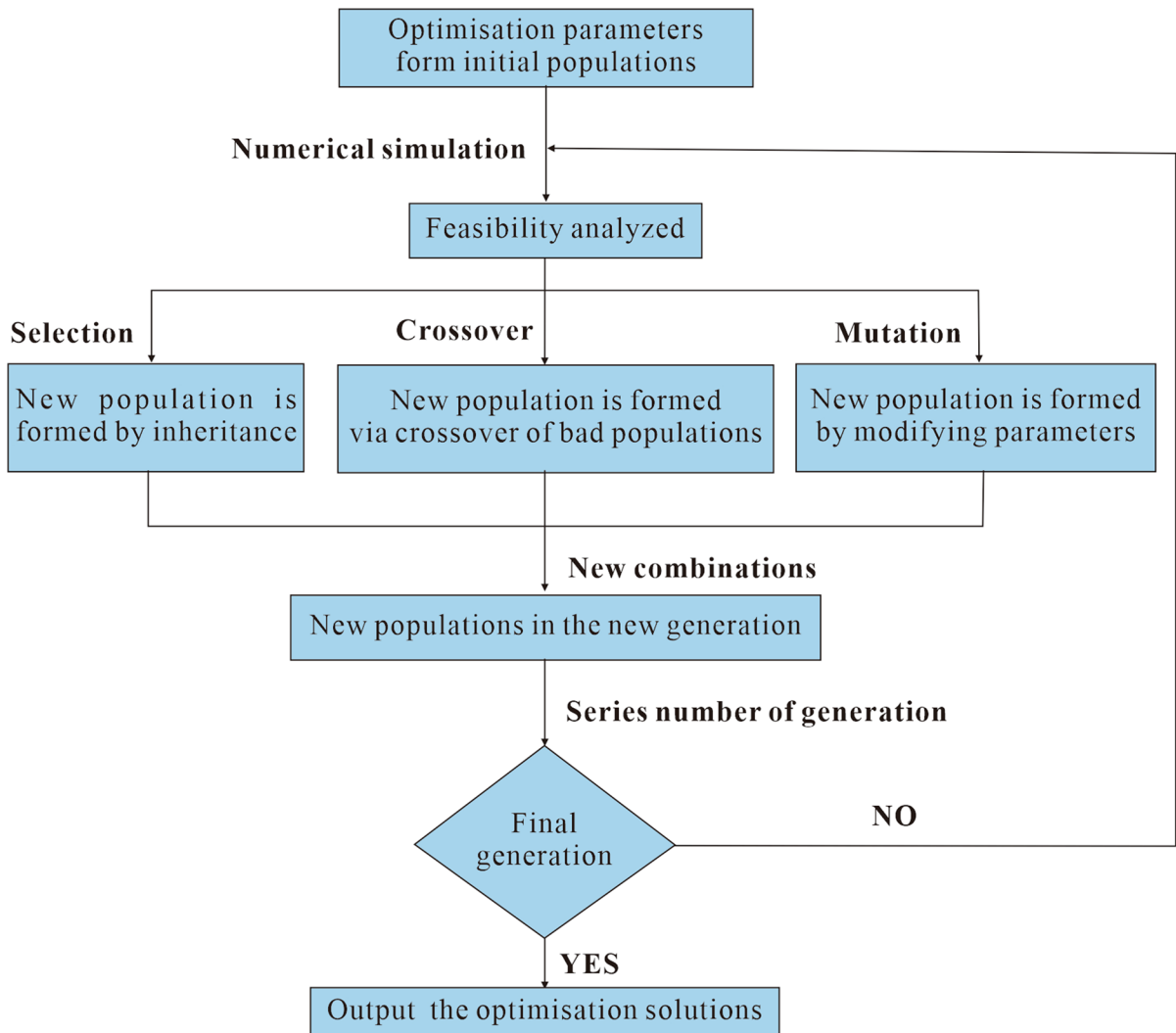


Fig. 4 Flow chart of the NSGA-II algorithm

is set as 90%, and the mutation distribution index is set as 10. The optimisation parameters vary between their lower and upper boundaries, as examples, the variations of six optimisation parameters are depicted in every 10 points in Fig. 5.

Finally, the obtained optimisation result is displayed in Fig. 6. As observed in subplot (a), the dynamic responses of the simulated cases satisfying all the three constraint conditions are depicted as blue points, specifically, the average moving speed of capsule remains between 6 and 8 mm/s, the average energy consumption is less than 0.02 W, and the maximal impact force is less than 0.1 N.

Furthermore, the optimisation parameter combinations suggested by NSGA-II are depicted as green points, which are selected from all the blue points. While the red points represent the simulation cases whose dynamic responses go beyond at least one of the three constraint conditions; hence, their corresponding parameter combinations should be avoided during capsule design. In addition, based on the distribution of the red points, the requirement of the average moving speed of capsule is hard to be controlled between 6 and 10 mm/s, since the average moving speeds of capsule for a large number of simulation cases are less than 6 mm/s. Although, for

Table 3 Optimisation ranges of structure and control parameters

Parameters	Units	Lower boundary	Upper boundary
m_1	kg	1×10^{-3}	5×10^{-3}
m_2	kg	1×10^{-3}	5×10^{-3}
k	N/m	20	90
k_1	N/m	20,000	50,000
k_2	N/m	40,000	80,000
e	m	0	2×10^{-3}
e_1	m	0	3×10^{-3}
e_2	m	0	3×10^{-3}
c	N s/m	5×10^{-3}	40×10^{-3}
R_s	Ω	0.5	0.9
P_d	N	2×10^{-3}	10×10^{-3}
f	Hz	10	80
d	%	20	90

some simulation cases, the average moving speed of capsule can be faster than 10 mm/s, the corresponding maximal impact force and/or the average energy consumption also increase to overcome their upper boundaries. Due to the existence of such contradictions among different optimisation objectives, the multi-objective optimisation algorithm should be

applied, since it can explore the optimal solutions via the compromise of contradictory optimisation objectives.

In order to intuitively observe the success rate of each optimisation objective, the bar charts are drawn in Fig. 6b–d. Specifically, the success rate of P_{avg} reaches a relatively high level as 74.6%, since according to Eq. 13, P_{avg} is only determined by P_d , d , and R_s , and the variations of other 10 optimisation parameters have no influence on it, hence the success rate of P_{avg} is secured once the relevant three parameters have been designed properly. Comparatively, the optimisation success rate of V_c is only 4.36%, since, as shown in Fig. 3, V_c is extensively affected by variety of optimisation parameters, and no parameter can mainly dominate the variation of V_c . Under such circumstances, the distribution of V_c cannot concentrate when the optimisation parameters vary, and thus the optimisation success rate of V_c decreases. In addition, the optimisation success rate of f_{max} is 72.5%, which cannot achieve higher success rate due to the basic requirement of V_c . Since the average moving speed of capsule should be remained between 6 and 10 mm/s to complete the endoscopy in 20 min, in order to achieve the required speed, the impact force which is used to drive the capsule cannot be too small.

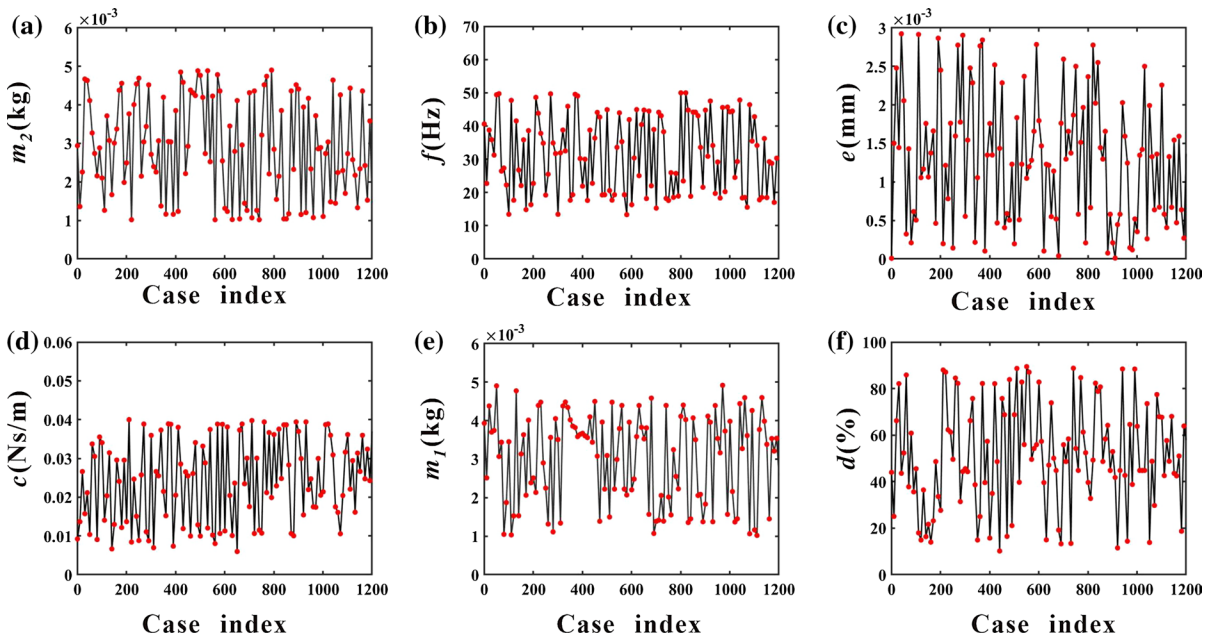


Fig. 5 Variation of optimisation parameters during preliminary multi-objective optimisation

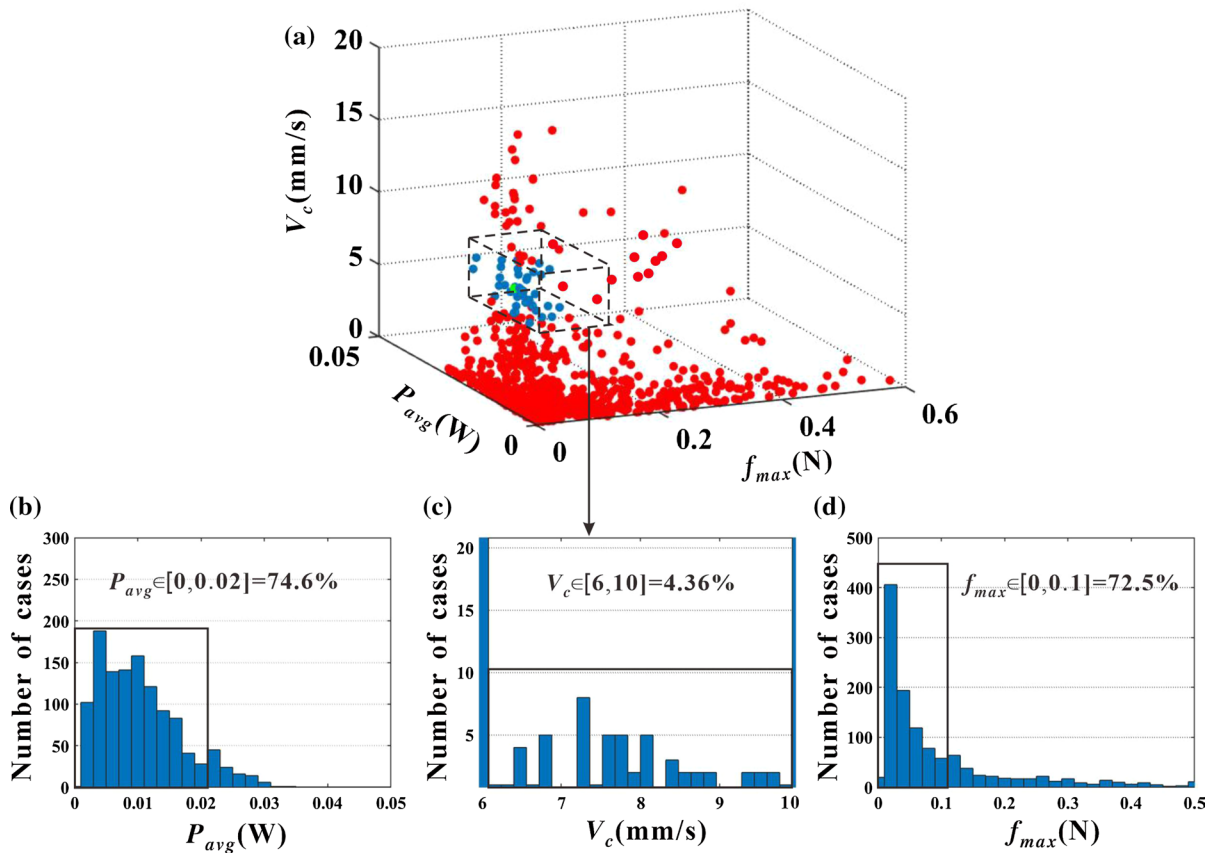


Fig. 6 Results of preliminary multi-objective optimisation. Subplot **a** show the distribution of dynamic responses about the three optimisation objectives, the red points represent the simulation cases whose dynamic responses go beyond at least one of the constraint boundaries of the three optimisation

objectives, while the blue points satisfy all the three optimisation objectives. Subplots **b–d** show the corresponding success rate for the optimisation objectives P_{avg} , V_c , and f_{max} , respectively. (Color figure online)

4.2 Verification of reliability

As is well known, all the optimal solutions obtained by NSGA-II are the feasible combinations of optimisation parameters from only the perspective of mathematics, and a part of the optimal solutions is close to the constraint boundaries; under such circumstances, once the optimisation parameters or the environmental parameters fluctuate slightly, the optimal solutions may jump across the constraint boundaries and lose the feasibility. In order to demonstrate such an idea, the reliability of one of the obtained optimal solutions is tested, whose parameters are listed in Table 4, and its $f_{max} = 0.017$ N, $P_{avg} = 0.01$ W, and $V_c = 8.11$ mm/s. During this verification of reliability, the friction coefficient varies around $\mu = 0.2293$ which was

set in the preliminary optimisation, and its variation range is $\pm 60\%$ to describe the variable small intestine environment. In addition, in order to take the design error or machining error into account, each optimisation parameter is allowed to vary within $\pm 5\%$ around its optimised value. Eventually, 800 groups of parameter fluctuations are determined by the Monte Carlo algorithm to test the reliability of this optimal solution.

In order to better observe the test result, the reliability for the capsule system satisfying the allowed range of each optimisation objective is calculated. As shown in Fig. 7a–c, the reliability of either f_{max} or P_{avg} is almost 100% although both the environmental parameter and the optimisation parameters fluctuate. However, the reliability of V_c is only 39.4%, which is

Table 4 Values of parameters obtained by preliminary multi-objective optimisation

Parameters	Units	Value
c	N s/m	3.81×10^{-2}
f	Hz	57.29
d	%	30.38
e	m	1.48×10^{-3}
e_1	m	2.76×10^{-4}
e_2	m	1.53×10^{-3}
k	N/m	62.88
k_1	N/m	26,123.74
k_2	N/m	51,070.00
m_1	kg	2.48×10^{-3}
m_2	kg	1.23×10^{-3}
P_d	N	8.52×10^{-3}
R_s	Ω	0.76

too low to be accepted for actual applications. Therefore, in order to secure the reliability of the obtained optimisation solutions, both the parameter perturbations and the environmental uncertainty should be considered accompanying with the optimisation, i.e.,

$$\begin{cases}
 X_L - \delta X \leq X \leq X_U + \delta X, \\
 Z_L \leq Z \leq Z_U, \\
 V_{cL} \leq G_1 = V_c(X, Z) + n\sigma_V(X, Z) \leq V_{cU}, \\
 f_{maxL} \leq G_2 = f_{max}(X, Z) + n\sigma_f(X, Z) \leq f_{maxU}, \\
 P_{avgL} \leq G_3 = P_{avg}(X, Z) + n\sigma_P(X, Z) \leq P_{avgU}, \\
 \text{Minimise } Y(V_a(X, Z), \sigma(X, Z)) = [(V_c(X, Z) - V_{cT})^2 - \sigma_V(X, Z)^2], \\
 \text{Minimise } Y(F_a(X, Z), \sigma(X, Z)) = [f_{max}(X, Z)^2 - \sigma_f(X, Z)^2], \\
 \text{Minimise } Y(P_a(X, Z), \sigma(X, Z)) = [P_{avg}(X, Z)^2 - \sigma_P(X, Z)^2],
 \end{cases} \tag{14}$$

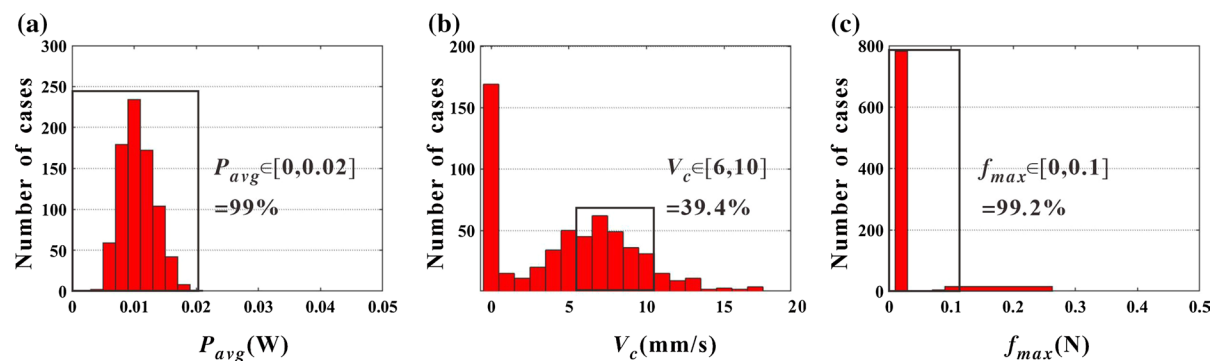


Fig. 7 Statistic results of reliability for **a** P_{avg} , **b** V_c , and **c** f_{max}

the multi-objective optimisation should be combined with the reliability analysis to secure all the obtained optimal solutions remaining a relatively high reliability even under the parameter fluctuations.

5 Multi-objective optimisation based on reliability analysis

5.1 Optimisation modelling

In order to take the reliability analysis into the multi-objective optimisation, a combination of algorithms is applied. The detailed combination procedure is illustrated in Fig. 8.

In the reliability optimisation, NSGA-II is still chosen to conduct the multi-objective optimisation, the Monte Carlo algorithm is also applied to measure the degree of reliability of the optimal solution explored by NSGA-II. In addition, the Six-Sigma algorithm is introduced to control the promotion of reliability of the obtained optimal solution, to extract the high reliable combinations of optimisation parameters. The corresponding optimisation model can be summarised as

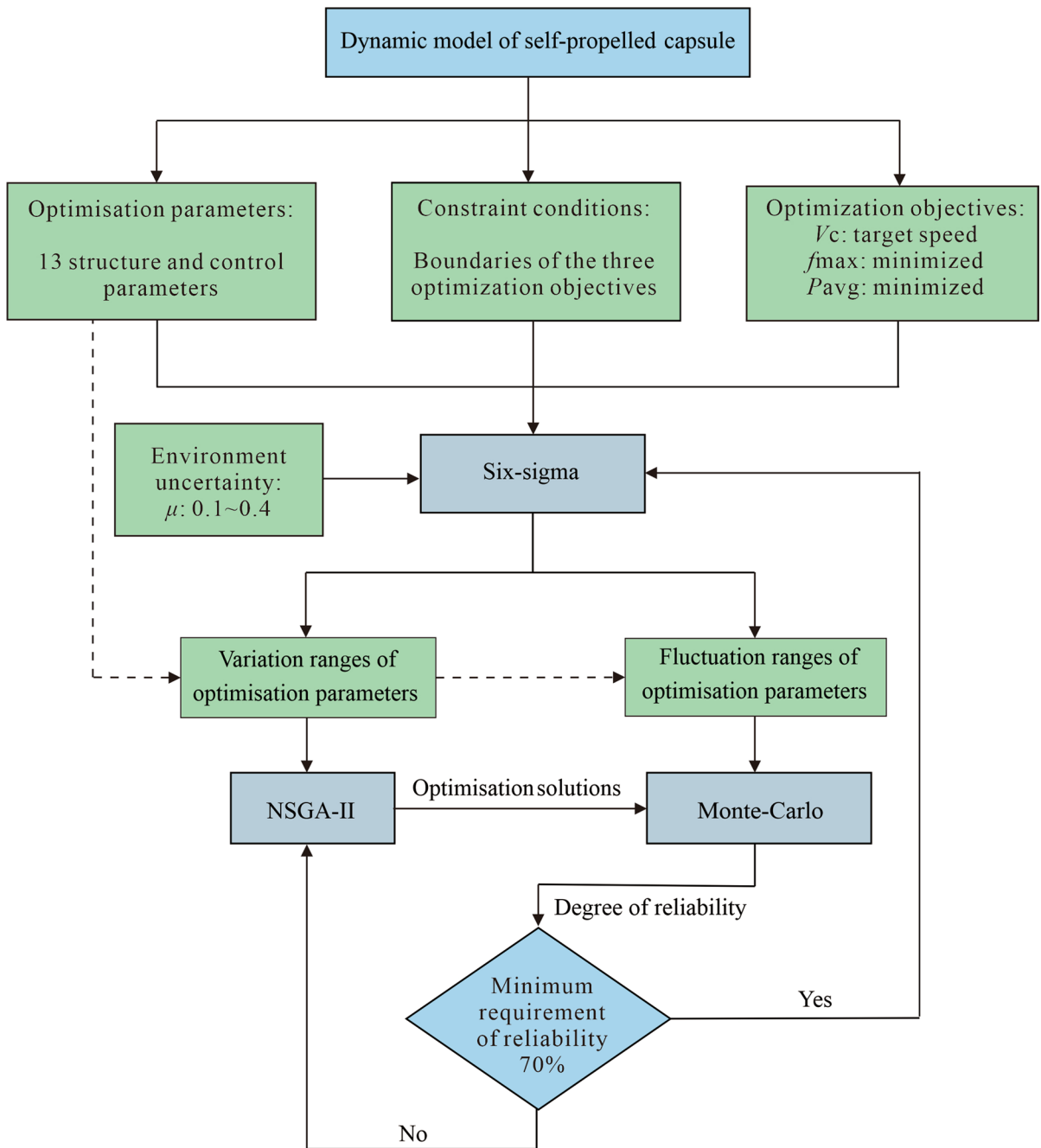


Fig. 8 Flow chart of multi-objective optimisation with reliability analysis of the self-propelled capsule system

where X represent the optimisation parameters, X_L , X_U , and δX are the lower and upper limits and the perturbations of the optimisation parameters, respectively. Z represents the friction coefficient, where Z_L and Z_U are its lower and upper limits, respectively,

and thus the uncertainty of the small intestine environment is taken into consideration. $G_i, i = 1, 2, 3$ represents the constraint condition, which sets the accepted variation range of each optimisation objective. $V_c(X, Z)$, $f_{max}(X, Z)$ and $P_{avg}(X, Z)$ are the

average moving speed of capsule, the maximal impact force, and the average energy consumption obtained from the dynamic responses of the self-propelled capsule system, respectively; $\sigma_V(X, Z)$, $\sigma_F(X, Z)$, and $\sigma_P(X, Z)$ are their corresponding standard deviations, respectively. In particular, n represents the number of sigma, when n is set as 6, the reliability of the optimisation solution needs to meet the highest level, hence this method is called as the Six-Sigma algorithm. Y represents the objective function, in which V_{c_T} is the target moving speed of capsule. With such an optimisation model, the capsule will be optimised to move with a speed close to the target value; meanwhile, the slight impact force and the low energy consumption are also expected to be achieved simultaneously.

5.2 Reliability optimisation for forward motion

In regard to reliability optimisation, in addition to the optimisation parameters, optimisation objectives, and constraint conditions, which are the three basic elements of optimisation, another key index, which should be set before reliability optimisation, is the lowest requirement of reliability of the obtained optimal solutions. In this study case, when considering the difficulty in maintaining the high speed of capsule, the lowest requirement of reliability is set as 70%. Subsequently, the reliability optimisation is carried out based on the developed optimisation model, and the obtained optimisation result is shown in Fig. 9. Comparing with the result of the multi-objective optimisation without reliability analysis

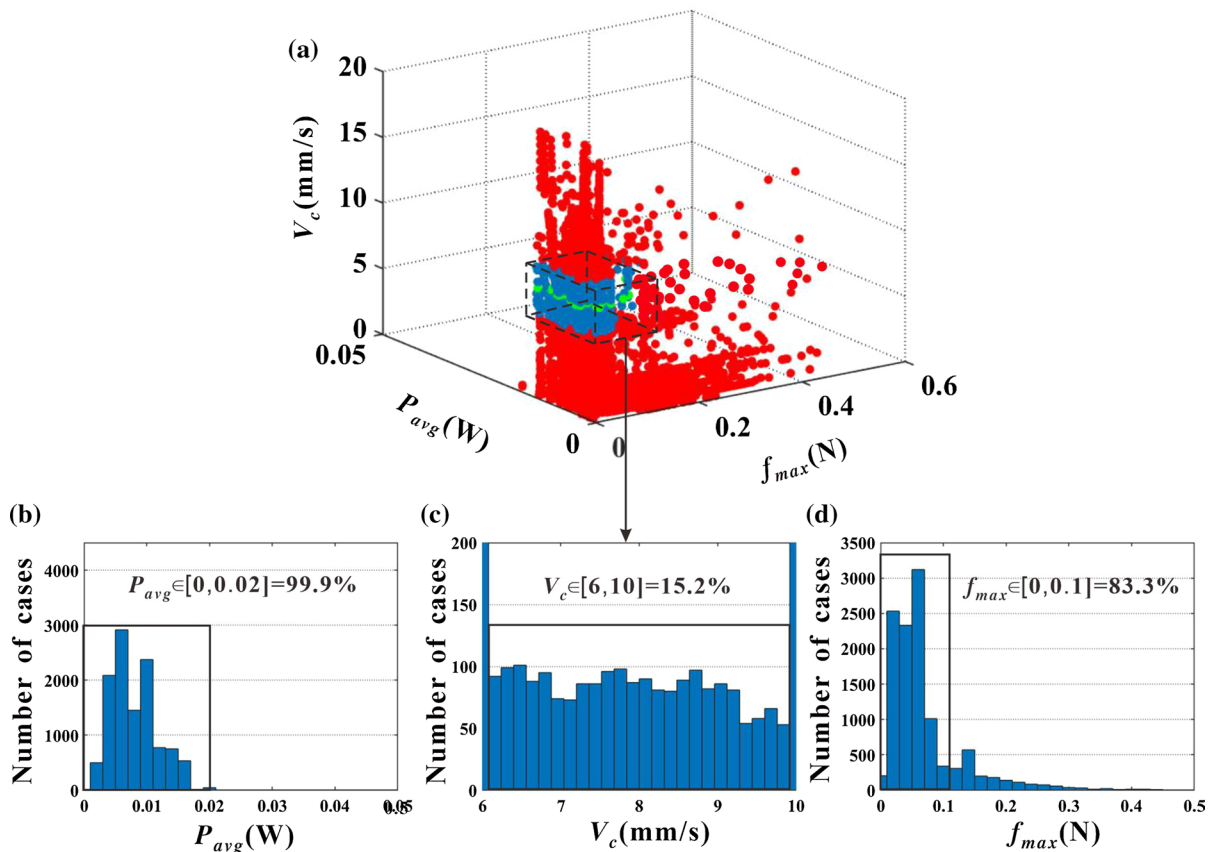


Fig. 9 Results of reliability optimisation for the forward motion of capsule. Subplot **a** show the distribution of dynamic responses about the three optimisation objectives, the red points represent the simulation cases whose dynamic responses go beyond at least one of the constraint boundaries of the three

optimisation objectives, while the blue points satisfy all the three optimisation objectives. Subplots **b–d** show the corresponding success rates for the optimisation objectives P_{avg} , V_c , and f_{max} , respectively. (Color figure online)

which is shown in Fig. 6, more optimisation solutions are explored via the reliability optimisation. Specifically, the high success rates of both P_{avg} and f_{max} are still remained, while the optimisation success rate of V_c increases from only 4.36% in Fig. 6c to 15.2% in Fig. 9c, namely, more combinations of optimisation parameters can make the capsule move forward with $V_c \in [6, 10]$ when both P_{avg} and f_{max} are minimised under the uncertain small intestine environment.

Since a number of optimal solutions have been explored, the following step is to extract the ranges of their corresponding optimisation parameters, which can be applied to guide the design and control of the self-propelled capsule. For each optimisation objective, the first three optimisation parameters

that have great impact on it, see Fig. 3, are analysed mutually. Specifically, based on all the obtained simulation cases during the reliability optimisation, the optimised regions in the parameter planes are determined by using the neural network fitting, and the results are shown in Fig. 10. By this way, the interactions between different optimisation parameters on the three optimisation objectives can be clarified. As observed from Fig. 10a–i, the red points represent the simulation cases conducted in reliability optimisation, and the lightened regions are the explored parameter regions that can meet all the three optimisation objectives; while the dark regions indicate that at least one of the optimisation objectives cannot be achieved. As observed, the lightened regions are scattered, and all

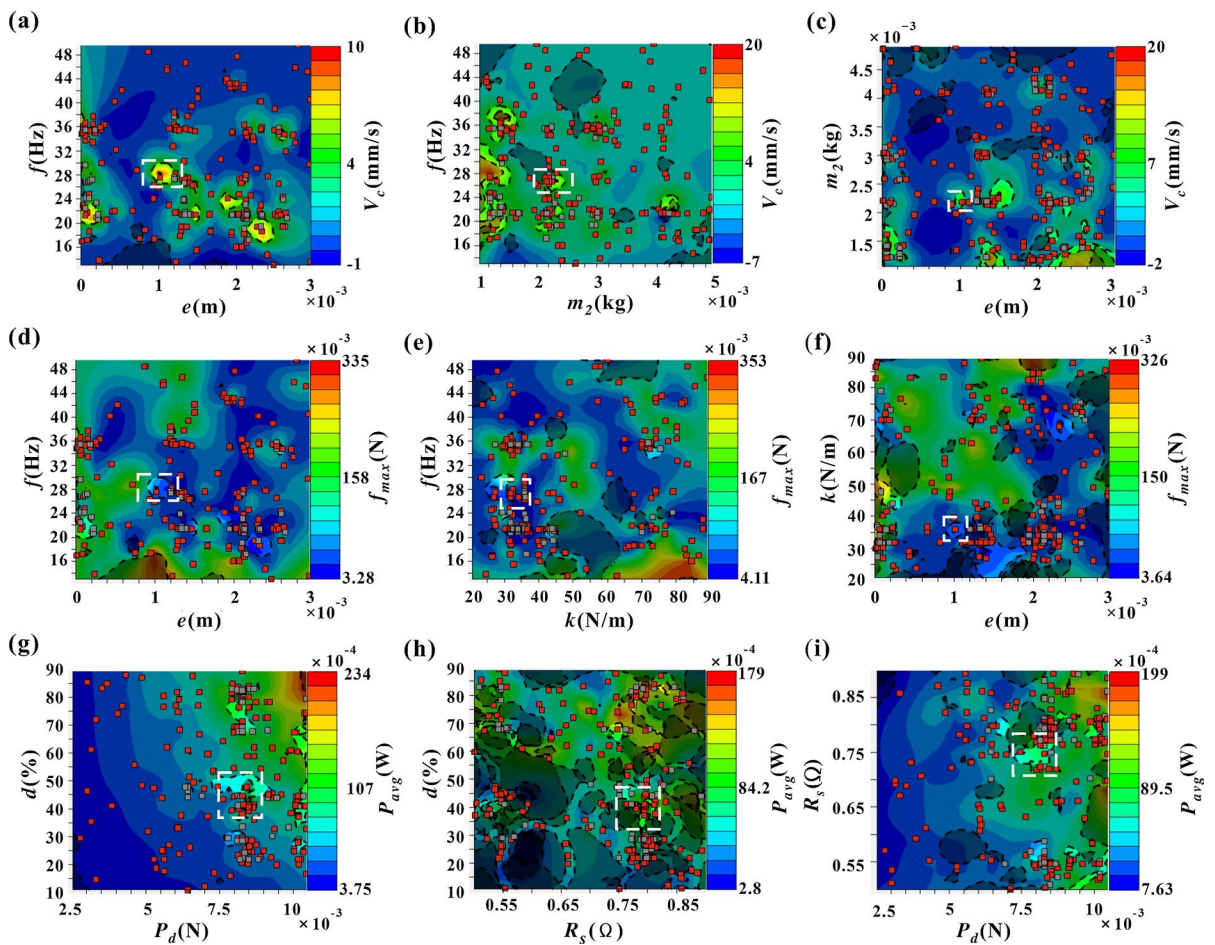


Fig. 10 (Color online) Distributions of V_c in subplots a–c, the maximal impact force f_{max} in subplots d–f, and P_{avg} in subplots g–i. The red points represent the simulated cases during reliability optimisation, the lightened regions are the explored

parameter ranges satisfying all the constraint boundaries, and the white dashed boxes indicate the suggested regions of optimisation parameters when considering all the three optimisation objectives at the same time. (Color figure online)

their regions are small, this is mainly determined by the target moving speed of capsule 8 mm/s, since it is not easy for the self-propelled capsule to remain such a high speed in the uncertain small intestine environment.

As shown in Fig. 10a–c, the interactions among the mass of capsule shell m_2 , the excitation frequency f , and the precompression of adjusting spring e are analysed since they are the first three optimisation parameters that have great impact on V_c . By observing the lightened areas overlapped in all the subplots (a)–(c), the suggested ranges of these three parameters are $f \in [16 \text{ Hz}, 32 \text{ Hz}]$, $e \in [0.001 \text{ m}, 0.0025 \text{ m}]$ and $m_2 \in [0.001 \text{ kg}, 0.0025 \text{ kg}]$. In terms of the maximal impact force f_{max} , the same as V_c , both the excitation frequency f and the precompression of adjusting spring e are also its key parameters, while the stiffness of the adjusting spring is the third one. As shown subplots (d)–(f), the variations of both f and e are restricted by the optimisation objective of V_c ; hence, their feasible regions are squeezed sharply, and the corresponding lightened regions are as small as $f \in [24 \text{ Hz}, 30 \text{ Hz}]$, $e \in [0.0008 \text{ m}, 0.0012 \text{ m}]$, and $k \in [30 \text{ N/m}, 40 \text{ N/m}]$. Similarly, when considering the optimisation objective of P_{avg} , the suggested parameter ranges are confirmed as $P_d \in [0.0075 \text{ N}, 0.0085 \text{ N}]$, $d \in [30, 50]$ and $R_s \in [0.75 \Omega, 0.85 \Omega]$. Finally, when all the three optimisation objectives are considered simultaneously, the suggested ranges for the control parameters are $f \in [24 \text{ Hz}, 30 \text{ Hz}]$, $P_d \in [0.0075 \text{ N}, 0.0085 \text{ N}]$, $d \in [30, 50]$, and the key structure parameters are $e \in [0.0008 \text{ m}, 0.0012 \text{ m}]$, $k \in [30 \text{ N/m}, 40 \text{ N/m}]$, $m_2 \in [0.002 \text{ kg}, 0.0025 \text{ kg}]$, and $R_s \in [0.75 \Omega, 0.85 \Omega]$, which are marked by the white dashed boxes in all the subplots in Fig. 10.

5.3 Verification of reliability

Since the reliability analysis has been introduced into the multi-objective optimisation, all the obtained solutions are expected to be reliable even under the variations of both the environmental parameter and the optimisation parameters. In order to further verify it, one of the solutions obtained from the reliability optimisation is tested, and the corresponding values of its optimisation parameters are listed in Table 5, and its $f_{max} = 0.02 \text{ N}$, $P_{avg} = 0.0045 \text{ W}$, and $V_c = 7.82 \text{ mm/s}$. The same as Sect. 4.2, the friction coefficient varies within $[0.1, 0.4]$; and each optimisation

Table 5 Values of parameters obtained by reliability optimisation

Parameters	Units	Value
c	N s/m	6.72×10^{-3}
f	Hz	26.36
d	%	33.58
e	m	1.13×10^{-3}
e_1	m	6.17×10^{-5}
e_2	m	1.7×10^{-3}
k	N/m	33.99
k_1	N/m	24,310.58
k_2	N/m	61,678.34
m_1	kg	1.94×10^{-3}
m_2	kg	2.17×10^{-3}
P_d	N	7.78×10^{-3}
R_s	Ω	0.79

parameter is allowed to vary within $\pm 5\%$ around its optimised value. The basic requirement for the reliability is still set as 70%. Eventually, 800 groups of parameter fluctuations are determined by the Monte Carlo algorithm to test the reliability of this optimal solution. The statistic results of reliability for P_{avg} , V_c , and f_{max} are shown in Fig. 11. As observed, the reliabilities of both f_{max} and P_{avg} achieve 100%; meanwhile the reliability of V_c is also greater than 70%, which meets the lowest requirement of reliability. Therefore, the reliability optimisation is demonstrated to be effective to secure the reliability of the explored optimal solution.

6 Reliability optimisation for backward motion

Compared with the passive capsules which move in small intestine environment depending on its peristalsis, and only one direction motion is achieved, the bi-directional motion can be fulfilled by the self-propelled capsule via adjusting its control parameters, which is one of its basic advantages. By this way, the return endoscopy of some ignored suspected regions can be conducted via the backward motion of the capsule. For such a potential application, the reliability optimisation for the backward motion of capsule is further discussed in this section.

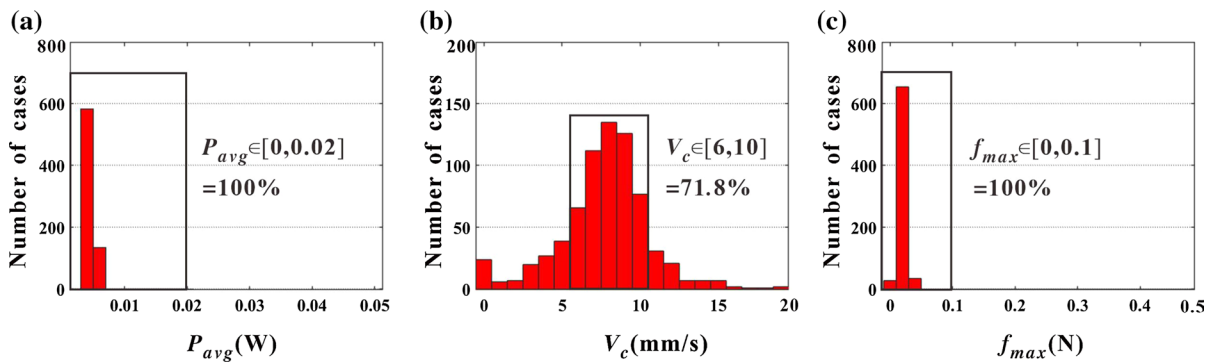


Fig. 11 Statistic results of reliability for **a** P_{avg} , **b** V_c , and **c** f_{max}

Table 6 Constraint conditions based on the three optimisation objectives for the backward motion of capsule

Optimisation objectives	Units	Target	Allowed range objectives
V_c	mm/s	-3	$[-4, -0.5]$
f_{max}	N	Minimum	$[0, 0.1]$
P_{avg}	W	Minimum	$[0, 0.02]$

6.1 Optimisation objectives and sensitivity analysis

Similar to the reliability optimisation for the forward motion, both the maximal impact force f_{max} and the average energy consumption P_{avg} should still be minimised, while V_c changes to be a negative value for backward motion. Under such circumstances, the corresponding constraint conditions based on the three optimisation objectives are listed in Table 6, while the variation range of optimisation parameters remains unchanged as shown in Table 3.

Based on the three optimisation objectives, the DOE algorithm is applied again to conduct the parameter sensitivity analysis of the backward motion of capsule, and the obtained results are shown in Fig. 12. Compared with the forward motion of capsule, the optimisation parameters that have great impact on V_c for the backward motion have changed from the previous m_2, f and e to the current m_2, m_1 and d , when the environmental parameter μ is excluded. Moreover, the contribution rates of these key parameters become more concentrated, such as $\mu = -20.57\%$, $m_2 = -17.6\%$, $m_1 = -16.34\%$, $d = 14.8\%$, and $P_d = 11.91\%$, while the contribution

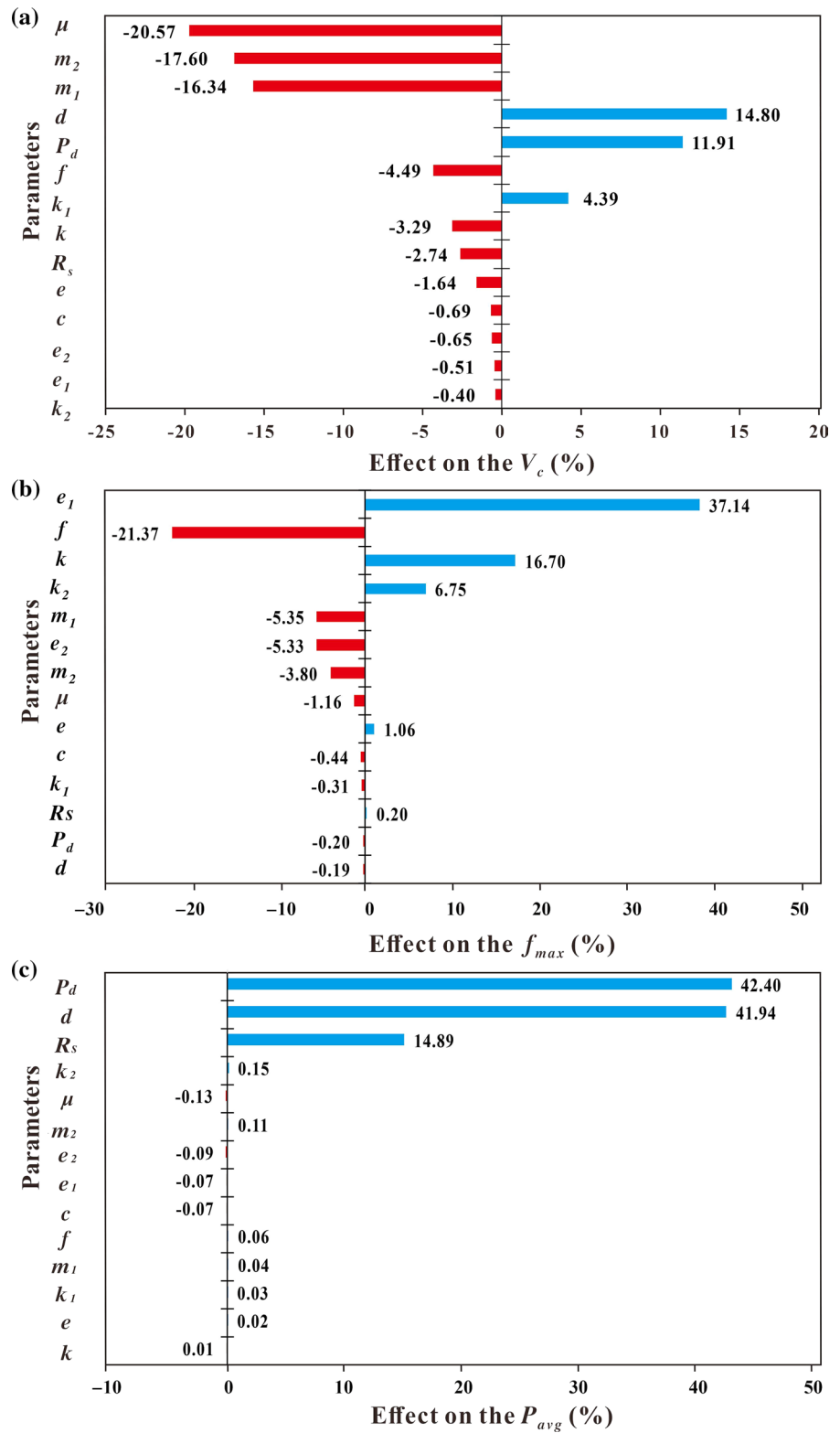
rates of other parameters are all lower than 5%. Due to the change of the moving direction of capsule, the primary influence parameter of f_{max} changes from e to e_1 , while the impacts of other parameters remain basically unchanged. In addition, P_{avg} for the backward motion of capsule owns the same parameter sensitivity as that of the forward motion of capsule.

6.2 Multi-objective optimisation based on reliability analysis

The optimisation process of the reliability optimisation for the backward motion of capsule is the same as that for its forward motion, and the obtained results are shown in Fig. 13. As observed in subplot (a), the low-speed backward motion of capsule can be achieved, however, it is difficult to achieve high-speed backward motion. Compared with the success rates of $P_{avg} = 100\%$ and $f_{max} = 89.8\%$, only 33.9% simulation cases enter into the allowed speed range $[-4 \text{ mm/s}, -0.5 \text{ mm/s}]$. Therefore, the control of the moving speed of capsule is still a challenge for the backward motion of capsule.

Subsequently, for each optimisation objective, the first three optimisation parameters that have the great impacts on it, see Fig. 12, are analysed mutually, and the optimised regions in the parameter planes are obtained by using the neural network fitting, and the results are shown in Fig. 14. When all the constraint conditions for the three optimisation objectives are considered simultaneously, the suggested ranges for the control parameters are $f \in [5 \text{ Hz}, 20 \text{ Hz}]$, $P_d \in [0.008 \text{ N}, 0.009 \text{ N}]$, $d \in [15, 25]$, and the key structure parameters are $e_1 \in [0.0005 \text{ m}, 0.001 \text{ m}]$, $k \in [20$

Fig. 12 Contribution rates of optimisation parameters on the optimisation objectives of **a** V_c , **b** f_{max} , and **c** P_{avg} for the backward motion of capsule; and the blue bars indicate the positive correlations, the red bars indicate the negative correlations. (Color figure online)



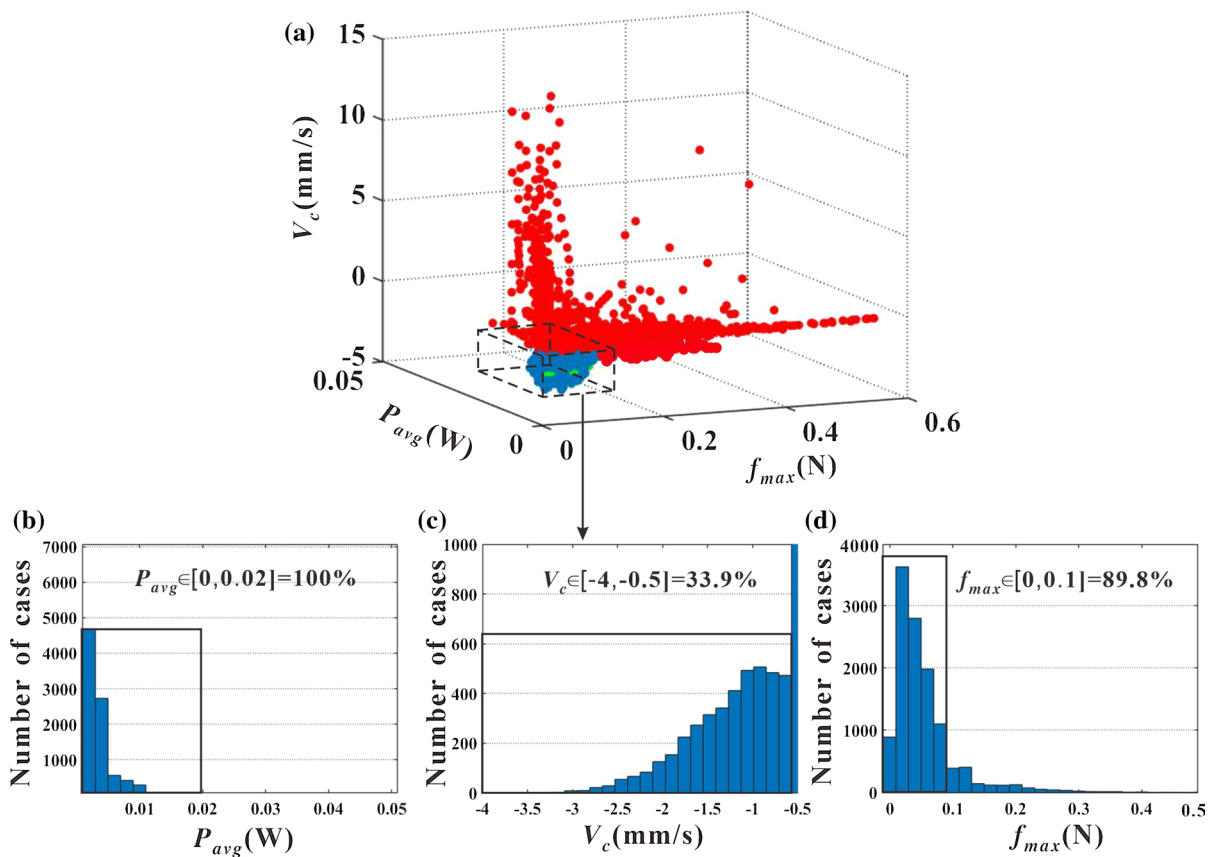


Fig. 13 Results of reliability optimisation for the backward motion of capsule. Subplot **a** show the distribution of dynamic responses about the three optimisation objectives, the red points represent the simulation cases whose dynamic responses go beyond at least one of the constraint boundaries of the three

optimisation objectives, while the blue points which are satisfy all the three optimisation objectives. Subplots **b–d** show the corresponding success rates for the optimisation objectives P_{avg} , V_c , and f_{max} , respectively. (Color figure online)

N/m, 30 N/m], $m_2 \in [0.0032 \text{ kg}, 0.0038 \text{ kg}]$, $m_1 \in [0.002 \text{ kg}, 0.0028 \text{ kg}]$, and $R_s \in [0.60 \Omega, 0.75 \Omega]$, which are marked by the white dashed boxes in all the subplots in Fig. 14.

6.3 Verification of reliability

In order to verify the reliability of the optimal solution for the backward motion of capsule, one of the solutions obtained from the reliability optimisation is further tested, and its corresponding values of optimisation parameters are listed in Table 7, and its $f_{max} = 0.05 \text{ N}$, $P_{avg} = 0.0038 \text{ W}$, and $V_c = -2.52 \text{ mm/s}$. During the verification of reliability, the friction coefficient μ varies within $[0.1, 0.4]$, and each optimisation parameter is allowed to vary within

$\pm 5\%$ around its optimised value. The basic requirement for the reliability is still set as 70%. Eventually, 800 groups of parameter fluctuations are determined by the Monte Carlo algorithm to test the reliability of this optimal solution. The statistic results of reliability for P_{avg} , V_c , and f_{max} are shown in Fig. 15. As observed, the reliabilities of both f_{max} and P_{avg} achieve 100%; while the reliability of V_c is 88.4%, which is greater than the lowest requirement of reliability 70%. Therefore, the reliability of this optimal solution is verified.

However, as shown in Fig. 15b, the results of V_c are mainly concentrated within $[-2 \text{ mm/s}, -0.5 \text{ mm/s}]$, and the target moving speed of capsule as -3 mm/s is hard to be achieved. As shown in Fig. 12a, as the environmental parameter, the

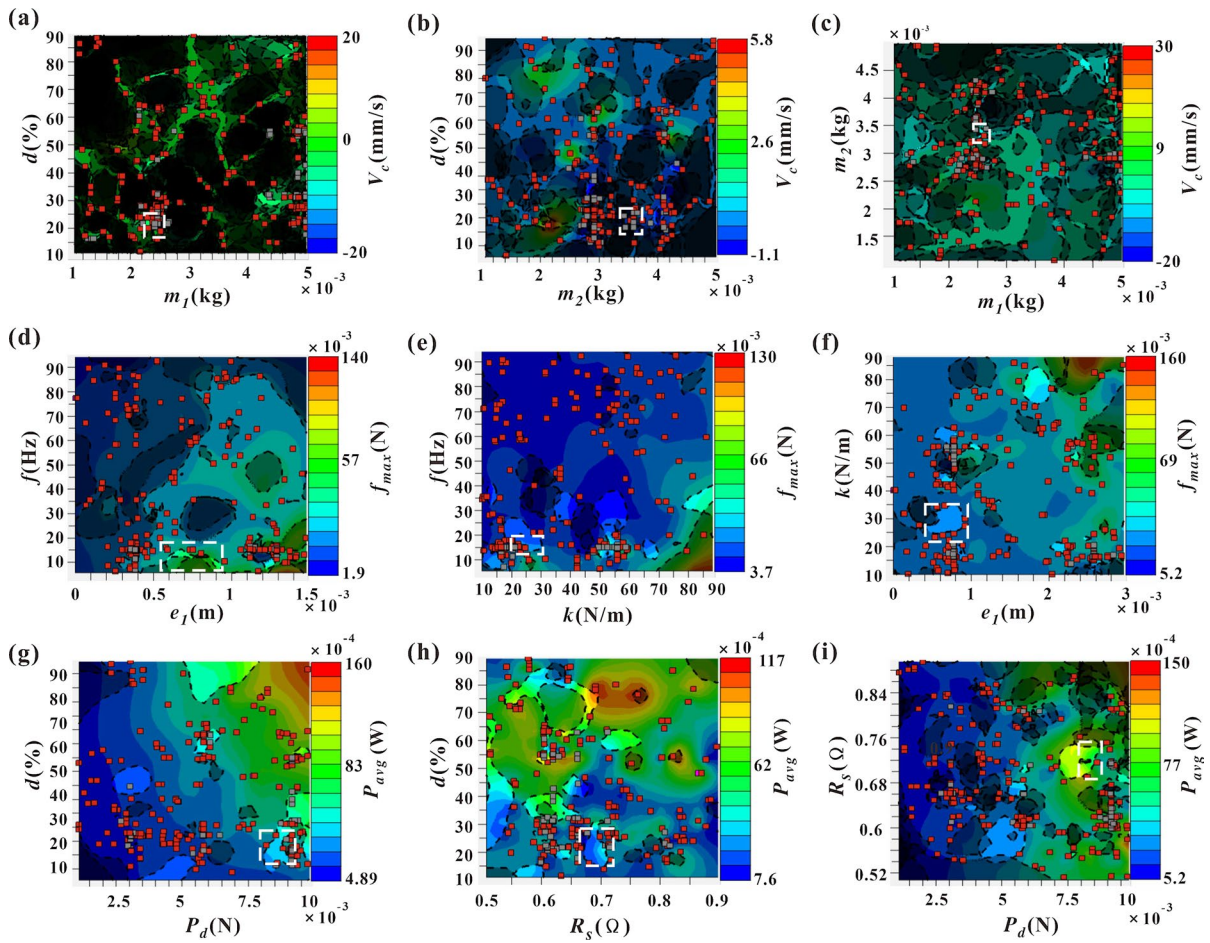


Fig. 14 (Color online) Distributions of V_c in subplots **a–c**, the maximal impact force f_{max} in subplots **d–f**, and P_{avg} in subplots **g–i** for the backward motion of capsule. The red points represent the simulated cases during reliability optimisation, the lightened regions are the explored parameter ranges satisfying

all the constraint boundaries, and the white dashed boxes indicate the suggested regions of optimisation parameters when considering all the three optimisation objectives at the same time

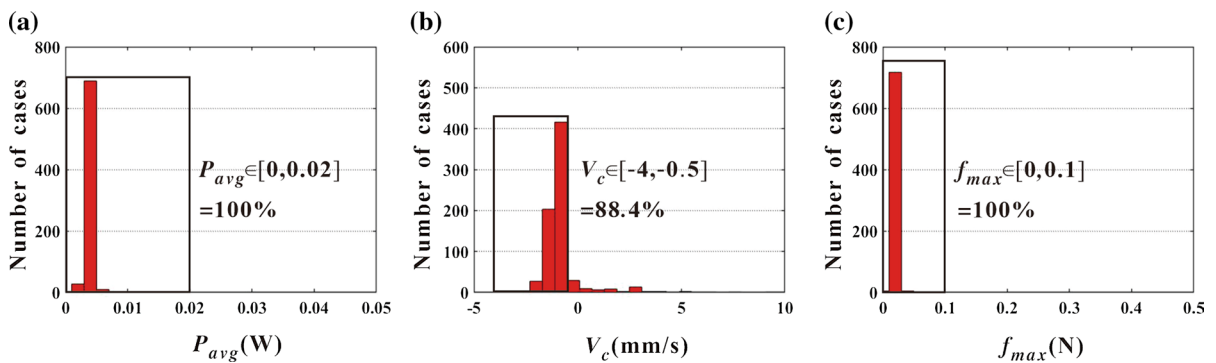


Fig. 15 Statistics of reliability for **a** P_{avg} , **b** V_c , and **c** f_{max} for the backward motion of capsule

Table 7 Values of parameters obtained by reliability optimisation for the backward motion of capsule

Parameters	Units	Value
c	N s/m	1.5×10^{-2}
f	Hz	15.29
d	%	21.68
e	m	3.58×10^{-4}
e_1	m	7.68×10^{-4}
e_2	m	7.29×10^{-4}
k	N/m	21.03
k_1	N/m	32,562.74
k_2	N/m	42,488.22
m_1	kg	2.6×10^{-3}
m_2	kg	3.4×10^{-3}
P_d	N	9.1×10^{-3}
R_s	Ω	0.63

friction coefficient μ has the largest negative effect on V_c , the increase of μ in the uncertain small intestine environment can considerably limit the acceleration of the self-propelled capsule in the backward direction; hence, the high-speed backward motion of capsule is hard to be achieved.

7 Concluding remarks

In the present work, the multi-objective optimisation with reliability analysis of a self-propelled capsule system was carried out. The minimum energy consumption, minimum impact force and the target moving speed of the capsule were taken as the multiple optimisation objectives; totally 13 optimisation parameters, including structure parameters and control parameters of the capsule system, were considered; the varied friction coefficient was applied to describe the uncertain small intestine environment where the capsule moving in. A combined optimisation method was employed, which consists of the Six-Sigma, NSGA-II, and Monte Carlo algorithms; based on which, the steady forward and backward motions of the capsule with the predefined progression speeds and the minimised impact force and energy consumption were fulfilled with high reliability.

Based on the massive numerical simulations during the optimisation, the forward motion of the self-propelled capsule with a large scale of moving

speed (from 0.1 to 15 mm/s) can be achieved via parameter adjustment; however, it is difficult for the capsule to achieve a high-speed backward motion. Generally, the obtained negative V_c was mainly concentrated within $[-2 \text{ mm/s}, -0.5 \text{ mm/s}]$; since, based on the sensitivity analysis, the friction coefficient μ has the strongest negative effect on the V_c when it moves backward, the increase influence of μ in the uncertain small intestine environment can considerably limit the acceleration of the self-propelled capsule in the backward direction.

According to the reliability analysis, for both the forward motion and the backward motion of the self-propelled capsule, the reliabilities of both the energy consumption and the impact force can reach 100% via reliability optimisations; however, the reliability of the target moving speed of capsule is relatively low, which is 71.8% for the forward motion and 88.4% for the backward motion. Comparing with the mature passive capsules applied clinically, which can move in the small intestine environment depending on its peristalsis, and only one direction motion can be achieved, the bi-directional motion can be fulfilled by the self-propelled capsule via adjusting its control parameters, which is one of its basic advantages. Although the reliability of the bi-directional motion of the capsule has been effectively improved, the reliability for the capsule moving with the target speed in the uncertain small intestine environment is still lower than 90%. Hence, how to further promote the moving reliability of the self-propelled capsule still needs to be studied.

Certainly, there are still a series of questions which need to be answered for the further application of the self-propelled capsule. For instance, the ranges of the three control parameters obtained by the reliability optimisations are different between the forward and backward motions, specifically, ($f \in [24 \text{ Hz}, 30 \text{ Hz}]$, $P_d \in [0.0075 \text{ N}, 0.0085 \text{ N}]$, $d \in [30, 50]$) for the forward motion, while ($f \in [5 \text{ Hz}, 20 \text{ Hz}]$, $P_d \in [0.008 \text{ N}, 0.009 \text{ N}]$, $d \in [15, 25]$) for the backward motion of capsule, which thus offer the confirmed control parameter combinations for the di-direction motion of the self-propelled capsule. However, some of the optimised structure parameters are also different between the forward and backward motions, for example, $m_2 \in [0.002 \text{ kg}, 0.0025 \text{ kg}]$ for the forward motion, while $m_2 \in$

[0.0032 kg, 0.0038 kg] for the backward motion, which will make the trouble in the structure design of the capsule, since the optimised mass of the capsule shell cannot be well-determined.

Acknowledgements Dr. Maolin Liao would like to acknowledge the financial support from Beijing Municipal Natural Science Foundation (No. 3204049), and from Interdisciplinary Research Project for Young Teachers of USTB (Fundamental Research Funds for the Central Universities) (No. FRF-IDRY-19-006).

Data availability The numerical data sets generated and analysed during the current study are available from the corresponding author on reasonable request.

Declarations

Conflict of interest The authors declare that they have no conflict of interest concerning the publication of this manuscript.

References

- Liu Y, Páez Chávez J, Zhang J, Tian J, Guo B, Prasad S (2020) The vibro-impact capsule system in millimetre scale: numerical optimisation and experimental verification. *Meccanica* 55:1885–1902
- Guo B, Ley E, Tian J, Zhang J, Liu Y, Prasad S (2020) Experimental and numerical studies of intestinal frictions for propulsive force optimisation of a vibro-impact capsule system. *Nonlinear Dyn* 101:65–83
- Guo B, Liu Y, Birlir R, Prasad S (2020) Self-propelled capsule endoscopy for small-bowel examination: proof-of-concept and model verification. *Int J Mech Sci* 174:105506
- Zhou H, Alici G (2019) A novel magnetic anchoring system for wireless capsule endoscopes operating within the gastrointestinal tract. *IEEE-ASME Trans Mech* 24:1106–1116
- Gao J, Zhang Z, Yan G (2020) Locomotion analysis of a clamper-based capsule robot in a compliant tube. *IEEE-ASME Trans Mech* 26(1):55–65
- Yan Y, Liu Y, Liao M (2017) A comparative study of the vibro-impact capsule systems with one-sided and two-sided constraints. *Nonlinear Dyn* 89(2):1063–1087
- Liao M (2020) Nonlinear dynamic behavior of impact capsule oscillator based on wireless endoscope application. *J Vib Shock* 39(23):279–286
- Tian J, Liu Y, Chen J, Guo B, Prasad S (2021) Finite element analysis of a self-propelled capsule robot moving in the small intestine. *Int J Mech Sci* 206:106621
- Yan Y, Liu Y, Jiang H, Peng Z, Crawford A, Williamson J, Thomson J, Kerins G, Yusupov A, Islam S (2019) Optimization and experimental verification of the vibro-impact capsule system in fluid pipeline. *Proc Inst Mech Eng C* 233(3):880–894
- Ing J, Pavlovskaja E, Wiercigroch M, Banerjee S (2008) Bifurcation analysis of an impact oscillator with a one-sided elastic constraint near grazing. *Physica D* 310:769–775
- Liao M, Liu Y, Páez Chávez J, Chong ASE, Wiercigroch M, Wiercigroch M (2018) Dynamics of vibro-impact drilling with linear and nonlinear rock. *Int J Mech Sci* 146:200–210
- Liao M, Ing J, Páez Chávez J, Wiercigroch M (2016) Bifurcation techniques for stiffness identification of an impact oscillator. *Commun Nonlinear Sci Numer Simul* 41:19–31
- Liao M, Ing J, Sayah M, Wiercigroch M (2016) Dynamic method of stiffness identification in impacting systems for percussive drilling applications. *Mech Syst Signal Process* 80:224–244
- Liao M, Wiercigroch M, Sayah M, Ing J (2021) Experimental verification of the percussive drilling model. *Mech Syst Signal Process* 146:107067
- Guo B, Chávez JP, Liu Y, Liu C (2021) Discontinuity-induced bifurcations in a piecewise-smooth capsule system with bidirectional drifts. *Commun Nonlinear Sci Numer Simul* 102:105909
- Guo SPB, Liu Y (2019) Modelling of capsule–intestine contact for a self-propelled capsule robot via experimental and numerical investigation. *Nonlinear Dyn* 98:3155–3167
- Liu Y, Páez Chávez J, Zhang BGSPJ, Tian J (2020) The vibro-impact capsule system in millimetre scale: numerical optimisation and experimental verification. *Meccanica* 55:1885–1902
- Jiang Z, Xu J (2017) Analysis of worm-like locomotion driven by the sine-squared strain wave in a linear viscous medium. *Mech Res Commun* 85:33–44
- Zhan X, Xu J, Fang H (2018) A vibration-driven planar locomotion robot-shell. *Robotica* 36(9):1402–1420
- Zhang Q, Fang H, Xu J (2021) Yoshimura–Origami based earthworm-like robot with 3-dimensional locomotion capability. *Front Robot AI* 8:056012
- Van der Velden A (2010) Isight design optimization methodologies. In: *ASM handbook*. ASM International, Materials Park
- Chen X, Yu X, Ji B (2010) Study of crankshaft strength based on Isight platform and DOE methods. *IEEE Comput Soc* 3(3):548–551
- Yin B, Xu D, An Y, Chen Y (2008) Aerodynamic optimization of 3D wing based on Isight. *Appl Math Mech* 29(5):603–610
- Koch PN, Evans JP, Powell D (2002) Interdigitation for effective design space exploration using Isight. *Struct Multidiscip Optim* 23(2):111–126
- Baril C, Yacout S, Clement B (2011) Design for Six Sigma through collaborative multi-objective optimization. *Comput Ind Eng* 60(1):43–55
- Asafuddoula M, Singh HK, Ray T (2015) Six-Sigma robust design optimization using a many-objective decomposition-based evolutionary algorithm. *IEEE Trans Evol Comput* 19(4):490–507
- Shirazi B, Fazlollahtabar H, Mahdavi I (2010) A six sigma based multi-objective optimization for machine grouping control in flexible cellular manufacturing systems with guide-path flexibility. *Adv Eng Softw* 41(6):865–873

28. Ray HSKAT, Asafuddoula M (2015) An approach to identify six-sigma robust solutions of multi/many-objective engineering design optimization problems. *J Mech Des* 137(5):051404
29. Zhang KCYWX, Lu Z (2020) A novel reliability sensitivity analysis method based on directional sampling and Monte Carlo simulation. *Proc Inst Mech Eng O* 234(4):622–635
30. Zhou L, Cai G, Yang J, Jia L (2010) Monte Carlo simulation based on FTA in reliability analysis of door system. In: *International conference on computer and automation engineering*, Singapore, Singapore
31. Li F, Brown RE, Freeman LAA (2003) A linear contribution factor model of distribution reliability indices and its applications in Monte Carlo simulation and sensitivity analysis. *IEEE Trans Power Syst* 18(3):1213–1215
32. Deb K, Pratap A, Agarwal S, Meyarivan T (2002) A fast and elitist multiobjective genetic algorithm: NSGA-II. *IEEE Trans Evol Comput* 6(2):182–197
33. Yusoff Y, Ngadiman M, Zain A (2011) Overview of NSGA-II for optimizing machining process parameters. *Procedia Eng* 15:3978–3983
34. Diao B, Zhang X, Fang H, Xu J (2021) Bi-objective optimization for improving the locomotion performance of the vibration-driven robot. *Arch Appl Mech* 91(5):2073–2088
35. Zhan X, Xu J, Fang H (2020) In-plane gait planning for earthworm-like metameric robots using genetic algorithm. *Bioinspir Biomim* 15:056012

Publisher's Note Springer Nature remains neutral with regard to jurisdictional claims in published maps and institutional affiliations.